Ionics (2014) 20:809–815
DOI 10.1007/s11581-013-1043-6

ORIGINAL PAPER

Effect of Mn doping on electrochemical properties of Li_2FeSiO_4/C cathode materials based on a vacuum solid-state method

Kun Gao

Received: 31 October 2013 / Revised: 14 November 2013 / Accepted: 25 November 2013 / Published online: 11 December 2013

Abstract $Li_2Fe_{1-x}Mn_xSiO_4$/C (x=0, 0.1, 0.2, 0.3, 0.4, 0.5) are prepared by a vacuum solid-state reaction of SiO_2, $CH_3COOLi \cdot 2H_2O$, $FeC_2O_4 \cdot 2H_2O$, and $Mn(CH_3COO)_2 \cdot 4H_2O$. The crystalline structures, morphologies, and electrochemical performances are analyzed contrastively by X-ray diffraction (XRD), scanning electron microscopy, galvanostatic charging–discharging, and electrochemical impedance spectroscopy (EIS). The XRD and EIS results prove that Mn doping may be beneficial to the battery performances of Li_2FeSiO_4 materials, by reducing the crystallite sizes, decreasing transfer impedance (R_{ct}), and increasing Li-ion diffusion coefficient (D_{Li+}). However, the galvanostatic charge–discharge results indicate that only $Li_2Fe_{0.8}Mn_{0.2}SiO_4$/C shows the improved performance; its initial discharge capacity can reach to 190.7 mAh g^{-1}. All things considered, the increased impurities after Mn doping, decided by reference intensity ratio (RIR) method, seem to impose more negative effects on the $Li_2Fe_{1-x}Mn_xSiO_4$/C performances. Under this premises, the Mn-doped content is particularly important for Li_2FeSiO_4 materials prepared by the vacuum solid-state method.

Keywords Cathodes · Batteries · Charging/discharging · Doping

Introduction

Li_2FeSiO_4 has such advantages as abundant natural resources, low cost, non-toxicity, environmentally friendly, safety, and high stability. Unfortunately, just like $LiFePO_4$, Li_2FeSiO_4 also suffers from the inherent low electronic conductivity and the slow Li^+ diffusion kinetics [1, 2]. To solve these problems, carbon doping [3–5] and cationic substitution [6] are the common methods widely used by researchers. The former is mainly conducted by the increased conductivity and decreased crystallite sizes, thus to effectively improve the electrochemical performances of cathode materials, while the latter could decrease Li^+ transfer impedance and accelerate Li^+ diffusion by causing lattice defects. When the added cations with radius most close to that of the substituted ions are employed, the distortion of crystal structure is slight enough to maintain crystal stability during long charge–discharge course, especially at high rates. Therefore, cationic substitution can impose more essential influences on modified materials. To date, various doping elements such as Mg [7], Al [8], Cr [9], Zn/Cu/Ni [10], V [11], and Mn [12–15] have been tried to improve the properties of Li_2FeSiO_4. In these studies, Mn doping attracts more attention. This is because: Mn has a close atomic radius with Fe (117 and 116.5 pm), and it has been already confirmed that Mn can be doped well into the crystal structure of Li_2FeSiO_4. Especially, Mn doping could purposely improve the low theoretical capacity of Li_2FeSiO_4 (~166 mAh g^{-1}), limited by the delithiated reaction from Fe^{2+} to Fe^{3+}. Here, the typical Mn-doped reports are listed as follow: C. Deng et al. prepared $Li_2Fe_{1-x}Mn_xSiO_4$ (x=0, 0.3, 0.5, 0.7, 1) nanoparticles using a citric acid assisted sol–gel method [12]. Mn doping resulted in the higher redox potentials and larger first discharge capacity than sole Li_2FeSiO_4 but sacrificed their cycling performances. By comparison, the highest discharge capacity (~172 mAh g^{-1}) was obtained when x was equal to 0.5. Similarly, B. Shao et al. synthesized $Li_2Fe_xMn_{1-x}SiO_4$/C ($0 \le x \le 0.8$) nano-composite cathodes by a novel synthesis route, i.e., a combination of spray pyrolysis and wet ball milling followed by annealing, in which $Li_2Fe_{0.5}Mn_{0.5}SiO_4$/C has delivered the highest discharge capacity of 149 mAh g^{-1} and showed the best cycle ability [13].

K. Gao (✉)
School of Chemistry and Materials Science, Shanxi Normal University, Linfen 041004, China
e-mail: gaokun0451@163.com

However, for H. J. Guo's report in which a mechanical activation-solid-state method was employed, and the optimized ratio become 0.1 ($Li_2Fe_{0.9}Mn_{0.1}SiO_4/C$), which has an initial discharge capacity of 158.1 mAh g^{-1} and a capacity retention ratio of 94.3 % after 30 cycles [14]. Furthermore, the $Li_2Fe_{3/4}Mn_{1/4}SiO_4/C$, prepared by X. G. He et al. [15] by a modified sol–gel method, showed the best electrochemical performance, and the first discharge capacity at room temperature could reach to 201 mAh g^{-1}. Note that, in these study, the best appropriate ratio of Mn doping seem to be confused, possibly due to the used different methods and synthetic procedures.

Here, to simulate practical production, based on a vacuum solid-state method having been employed in our previous studies [16–18], we prepared $Li_2Fe_{1-x}Mn_xSiO_4/C$ composite materials with different amount of Mn doping under the same process conditions. The effects of Mn content on crystal structure, morphology, properties, and Li^+ diffusion coefficient were discussed. This work could provide valuable references for actual applications of high-quality Li_2FeSiO_4 cathodes.

Experimental

According to the chemical formula of Li_2Fe_{1-x} Mn_xSiO_4 (x=0, 0.1, 0.2, 0.3, 0.4, 0.5), the stoichiometric amount of analytical reagents, lithium acetate dehydrate, iron oxalate dehydrate, manganese acetate tetrahydrate, nano-silica, and 10 wt% mass of glucose monohydrate as carbon sources, were ground to fine powder together and then heated from room temperature to 700 °C for 10 h in a vacuum tube furnace keeping −0.1 MPa throughout. The final products were used as $Li_2Fe_{1-x}Mn_xSiO_4/C$ materials with the designed Mn content.

The $Li_2Fe_{1-x}Mn_xSiO_4$ crystal structures were analyzed by powder X-ray diffraction (Ultima IV, Rigaku) employing Cu $K_{\alpha 1}$ radiation (λ=0.154056 nm) in the two-theta range of 10–80°. The morphologies were observed using a field emission scanning electron microscope (FESEM; JSM-7500 F, Japan JEOL). Electrochemical experiments were performed using CR2016-type coin cells. The mixtures of $Li_2Fe_{1-x}Mn_xSiO_4/C$, acetylene black, and polyvinylidene fluoride with a weight ratio of 80:10:10 were used as the cathode. The $Li|LiPF_6$(EC + DMC)$|Li_2Fe_{1-x}Mn_xSiO_4/C$ cells were fabricated in an Ar-filled glove box and measured on a 5-V/2-mA battery-testing system (Land CT2001A, China Wuhan Jinnuo Electronics Co., Ltd.). The charge–discharge cycles were carried out at room temperature with cut-off voltage of 1.5–4.5 V under a constant current density of 10 mAh g^{-1}. The specific capacities were calculated based on the net mass of $Li_2Fe_{1-x}Mn_xSiO_4$. The AC impedance spectra were measured via an electrochemical workstation (CHI 604D, Shanghai CH Instruments, Inc.) in the frequency range from 0.1 Hz to 100 kHz with perturbation amplitude of 5 mV.

Results and discussion

XRD

Figure 1 compares X-ray diffraction (XRD) patterns of $Li_2Fe_{1-x}Mn_xSiO_4/C$ with different amount of Mn doping. The main characteristic peaks of all samples are similar and can be assigned to Li_2FeSiO_4 phase. All the samples have an orthorhombic structure (space group $Pmn2_1$) and similar lattice parameters. This result is consistent with the other reports [12, 14]. Furthermore, the semiquantitative XRD analysis with reference intensity ratio (RIR) method was used to roughly evaluate the samples' components. The obtained results, along with crystallite sizes calculated by Scherrer formula ($D=K\lambda/(B_{0.5}\cos\theta$, where D denotes crystallite size, K is Scherrer constant, λ is X-ray wavelength, $B_{0.5}$ is the peak width at half height and θ is diffraction angle) were shown in Table 1. Compared with original Li_2FeSiO_4, Mn doping results in the reduced crystallite sizes. Moreover, the proportions of active materials in the Mn-doped samples obviously decrease along with the significant increased MnO and Li_2SiO_3 impurities, except for $Li_2Fe_{0.8}Mn_{0.2}SiO_4$ sample, whose main phase content is of 83.6 %, close to that of Li_2FeSiO_4 synthesized by the same method. This result proves that the manganese salt may actively participate in the thermal reaction, and to some extent, increase the complexity of solid-phase reaction.

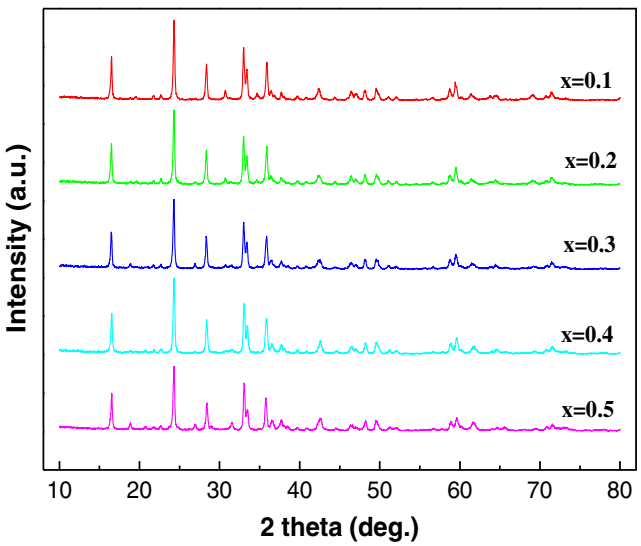

Fig. 1 XRD patterns of $Li_2Fe_{1-x}Mn_xSiO_4/C$ with different Mn content

Table 1 Summary of semiquantitative analysis and crystallite size based on XRD data

$Li_2Fe_{1-x}Mn_xSiO_4/C$	Weight percent concentration (wt%)				Crystallite sizes (nm)
	$Li_2Fe_{1-x}Mn_xSiO_4/C$	MnO	Li_2SiO_3	Fe_2O_3	
$x=0$	83.1	–	10.7	6.2	62.2
$x=0.1$	77.2	0.6	17.3	4.9	32.1
$x=0.2$	83.6	0.9	7.1	8.2	41.6
$x=0.3$	68.0	1.3	25.1	5.6	43.0
$x=0.4$	61.2	2.4	19.3	17.0	46.8
$x=0.5$	64.1	3.9	23.8	8.2	43.9

SEM

Figure 2 shows the scanning electron microscopy (SEM) photographs of $Li_2Fe_{1-x}Mn_xSiO_4/C$ with different amount of doped Mn. All the samples are made up of some irregular-shaped particles in various sizes, and the significant effect of Mn doping on the morphologies of final products are hardly ever observed. But it is obvious to notice that the particle sizes shown in Fig. 2 are relatively larger than crystallite sizes calculated by XRD data (~40 μm) because our observations from SEM photographs are the aggregates of single crystalline grains. This difference usually means serious aggregates of primary particles in these samples, which can be mainly attributed to the employed solid-state method.

Electrochemical performance

Figure 3 shows the typical charge–discharge curves of $Li_2Fe_{1-x}Mn_xSiO_4/Li$ coin cells at room temperature. By comparison, three key features should be noted.

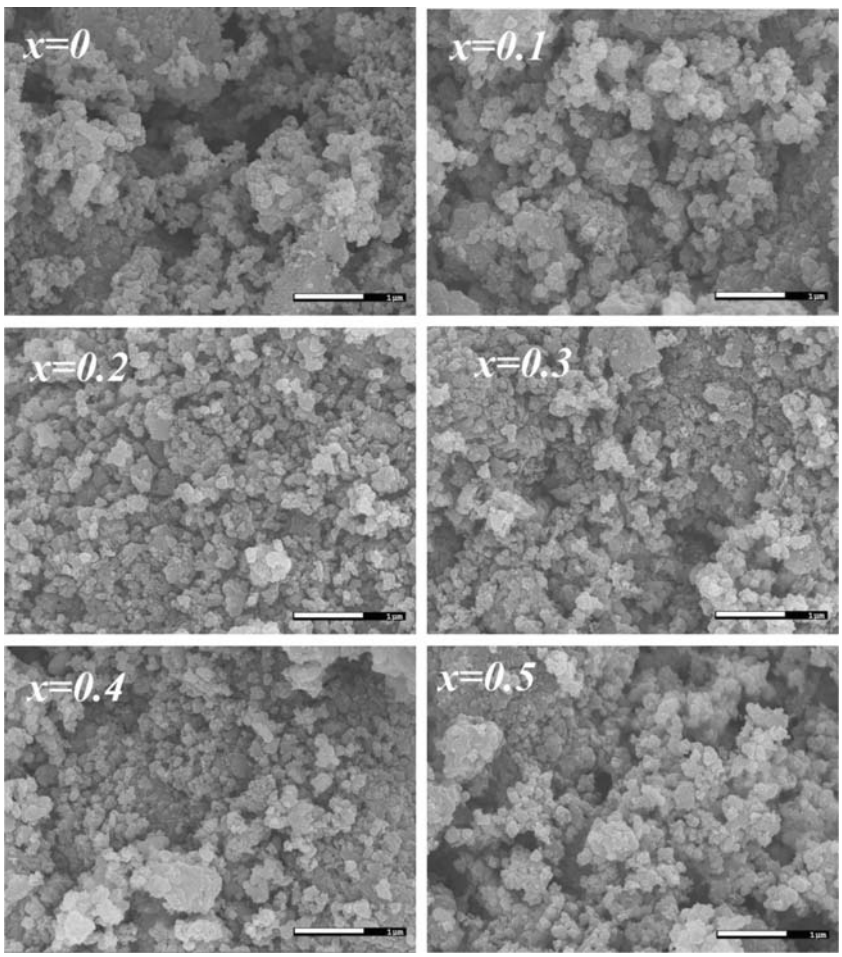

Fig. 2 SEM photographs of $Li_2Fe_{1-x}Mn_xSiO_4/C$ with different Mn content

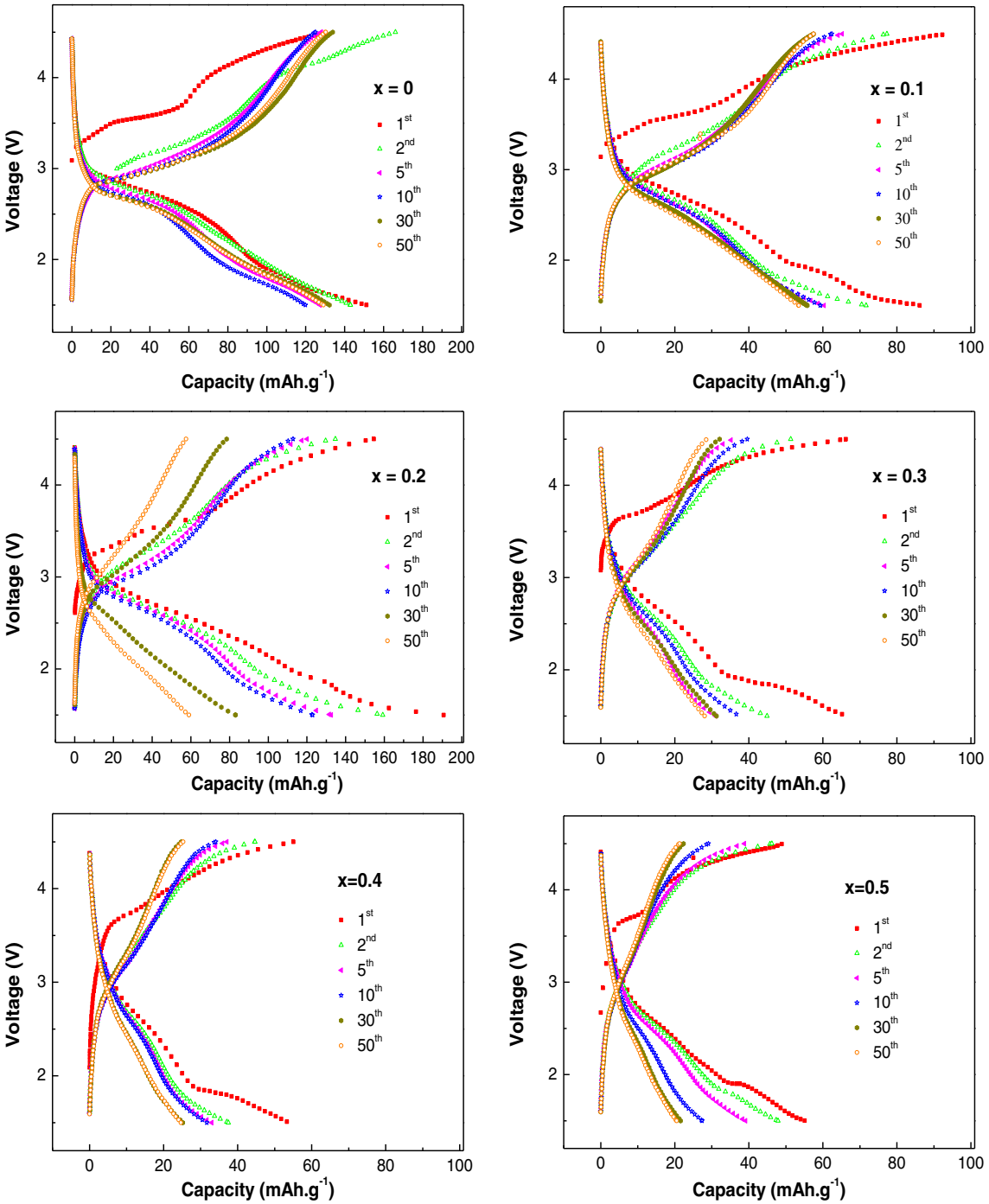

Fig. 3 Typical charge–discharge curves of $Li_2Fe_{1-x}Mn_xSiO_4/C$ with different Mn content

First, with the increased Mn content, the charge plateau at 3.5 V shortens and that above 4.0 V increases gradually. That is to say that Mn doping leads to a higher proportion for the plateau-like charge curve above 4.0 V. This phenomenon can be presented as evidence that the doped Mn can be involved in the delithiated reaction during charging. However, the first charge curves of all tested samples are still higher than the subsequent cycles, demonstrating that Mn doping does not prevent from the structural rearrangements of Li_2FeSiO_4 mainly occurred in the first several cycles [2, 17, 19].

Second, compared with Li_2FeSiO_4/C material, only $Li_2Fe_{0.8}Mn_{0.2}SiO_4/C$ shows higher specific capacity in all Mn-doped samples, and its initial discharge capacity can reach

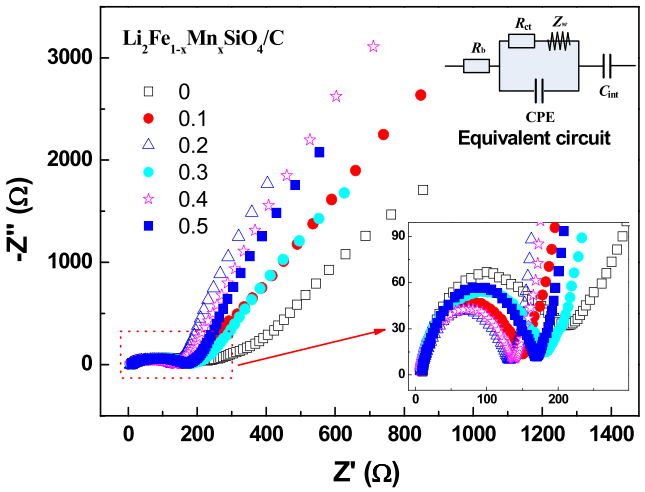

Fig. 4 Nyquist spectra and equivalent circuit of $Li_2Fe_{1-x}Mn_xSiO_4/C$ with different Mn content

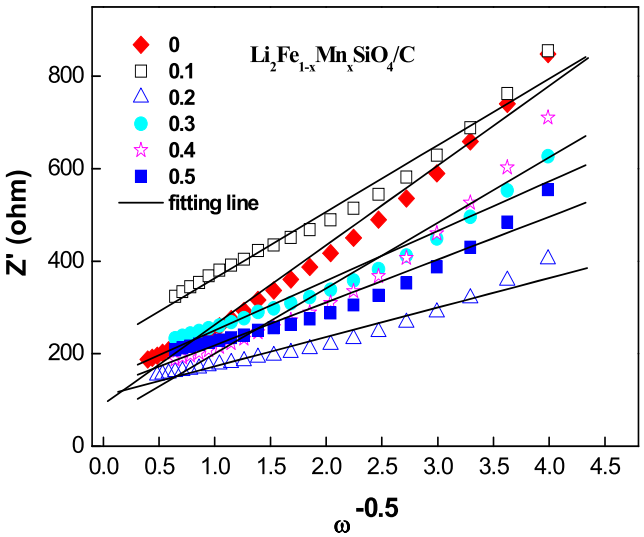

Fig. 5 Relationship curves between Z′ and $\omega^{-0.5}$ in the low frequency of $Li_2Fe_{1-x}Mn_xSiO_4$ with different Mn content

to 190.7 mAh g^{-1}. For this result, the negative influence of more impurities (see "XRD") can play a more important role.

Third, the Mn-doped cathodes (except for $x=0.1$ sample) show significant capacity loss after 50 cycles. Taking $Li_2Fe_{0.8}Mn_{0.2}SiO_4/C$ as an example, its discharge capacity at 50th cycle is down to 60 mAh g^{-1}, and the retention is only 31.5 % as compared to that at the first discharge. Many researchers attributed it to the crystal instability, mainly caused by Jahn–Teller effect of Mn^{3+} [12–15]. Thus, Mn doping can improve specific capacity but in most cases at the expense of cycling performance.

EIS

Figure 4 shows typical *Nyquist* impedance spectra of $Li_2Fe_{1-x}Mn_xSiO_4/Li$ coin cells after 2 cycles. The measured spectra all exhibit a semicircle in high frequency and a straight line in the low frequency. The high-frequency semicircle is related to the contact impedance between the electrode material and the electrolyte in the charge transfer process. The low-frequency straight line is associated with *Warburg* impedance of lithium ion diffusion in the electrode material. Furthermore, in the equivalent circuit shown at the top right corner in Fig. 4, R_b represents the bulk resistance; R_{ct} refers to the charge transfer resistance on the interface of electrode and electrolyte; Z_w represents the *Warburg* impedance caused by lithium ion diffusion in solid-phase electrode; CPE is a constant phase element, informing the degree of deviation of impedance behavior from capacity behavior; C_{int} represents the capacity reactance resulted from lithium ion accumulation and consumption in active materials.

From Table 2, we can see that the R_b values of all the tested samples are lightly different. It is acceptable for this due to the electrolyte usage amount, electrode piece position, sealing force, etc. during the process of manual assembly of coin cells. Note that compared with that of Li_2FeSiO_4/C, the R_{ct} of the Mn-doped materials decrease obviously, indicating that the Mn doping can lower the kinetic barriers of Li^+ transfer, accelerate the delithiation procedure, increase the electrochemical reaction kinetics, and improve the electrochemical performances of $Li_2Fe_{1-x}Mn_xSiO_4/C$. In addition, the decreased C_{int} values can be explained that the more effective Li^+ transfer can buffer the charge car-

Table 2 Fitting results based on EIS data

$Li_2Fe_{1-x}Mn_xSiO_4/C$	R_b (ohm cm^{-2})	R_{ct} (ohm cm^{-2})	C_{int} (F cm^{-2})	σ (ohm $s^{-0.5}$)	D_{Li+} (cm^2 s^{-1})
$x=0$	17.89	389.6	0.007789	143.92	6.83×10^{-17}
$x=0.1$	11.03	264.8	0.003417	172.20	4.77×10^{-17}
$x=0.2$	13.42	246.6	0.004787	63.68	3.49×10^{-16}
$x=0.3$	8.8	344.7	0.005742	107.40	1.23×10^{-16}
$x=0.4$	11.74	251.3	0.002703	141.59	7.05×10^{-17}
$x=0.5$	16.88	314.8	0.004119	92.62	1.65×10^{-16}

riers' accumulation and consumption in the local active materials.

The Li-ion diffusion coefficient (D_{Li+}) in active electrode can be calculated from the low-frequency plots according to the following equation [20–22]:

$$D_{Li+} = R^2T^2/\left(2A^2n^4F^4C^2\sigma^2\right) \quad (1)$$

where R is the gas constant, T is the absolute temperature, A is the surface area of the electrode, n is the number of electrons per molecule during oxidation, F is the Faraday constant, C is the concentration of lithium ion, and σ is the *Warburg* factor which is relative with Z':

$$Z' = B + \sigma\omega^{-0.5} \quad (2)$$

where B is a constant and ω is the frequency in low-frequency region. Therefore, σ can be decided by the slope of $\omega^{-0.5}$–Z' curve, as shown in Fig. 5. The calculated σ and D_{Li+} are both listed in Table 2. Comparison shows that all the Mn-doped materials (except for $x=0.1$ sample) have lightly increased D_{Li+} values, in which $Li_2Fe_{0.8}Mn_{0.2}SiO_4$/C sample shows a highest D_{Li+} value of 3.49×10^{-16} cm^2 s^{-1}. The results verify that the diffusion capability of lithium ion can be effectively improved by Mn doping.

Conclusion

Based on the above discussions, we can conclude that the Mn doping can bring some beneficial effects to improve the electrochemical performances of $Li_2Fe_{1-x}Mn_xSiO_4$/C products, such as reducing the crystallite sizes, decreasing the R_{ct} value, lowering the kinetic barriers of Li^+ transfer, increasing the D_{Li+} values, and so on. However, it also leads to a significant amount of impurities and serious aggregates in the final product, which is close related to the employed vacuum solid-state method. For this reason, the doped Mn content is more important to achieve the purpose of optimizing Li_2FeSiO_4 materials. Here, the $Li_2Fe_{0.8}Mn_{0.2}SiO_4$/C sample showed the highest initial discharge capacity of 190.7 mAh g^{-1}, which could be attributed to its less impurities and higher D_{Li+} values. Regrettably, it still showed obvious capacity fading, whose discharge capacity at 50th cycle dropped to 60 mAh g^{-1} only with the capacity retention of 32.5 %. Therefore, future researches should be mainly focused on overcoming this defect, aiming at strengthening the crystal stability of the Mn-doped materials and improving their long-cycle performances.

Acknowledgments This work was financially supported by National Natural Science Foundation of China (NSFC) (grant no. 21003087), Research Fund for the Doctoral Program of Higher Education (grant no.20101404120001), and China Postdoctoral Science Foundation (grant no. 20110491051).

References

1. Dominko R (2008) Li_2MSiO_4 (M = Fe and/or Mn) cathode materials. J Power Sources 184:462–468
2. Nytén A, Abouimrane A, Armand M, Gustafsson T, Thomas JO (2005) Electrochemical performance of Li_2FeSiO_4 as a new Li-battery cathode material. Electrochem Commun 7:156–160
3. Zhang S, Deng C, Yang SY (2009) Preparation of Nano-Li_2FeSiO_4 as Cathode Material for Lithium-Ion Batteries. Electrochem Solid-State Lett 12:A136–A139
4. Muraliganth T, Stroukoff KR, Manthiram A (2010) Microwave-Solvothermal Synthesis of Nanostructured Li_2MSiO_4/C (M = Mn and Fe) Cathodes for Lithium-Ion Batteries. Chem Mater 22:5754–5761
5. Dahbi M, Urbonaite S, Gustafsson T (2012) Combustion synthesis and electrochemical performance of Li_2FeSiO_4/C cathode material for lithium-ion batteries. J Power Sources 205:456–462
6. Islam MS, Dominko R, Masquelier C, Sirisopanaporn C, Armstrong AR, Bruce PG (2011) Silicate cathodes for lithium batteries: alternatives to phosphates? J Mater Chem 21:9811–9818
7. Zhang S, Deng C, Fu BL, Yang SY, Ma L (2010) Doping effects of magnesium on the electrochemical performance of Li_2FeSiO_4 for lithium ion batteries. J Electroanal Chem 644:150–154
8. Lan JY, Zhao MS, Wang YZ, Qiao YQ (2011) Effent of Al^{3+} doping on structure and electrochemical performance of Li_2FeSiO_4. Chin J Inorg Chem 27:1497–1502
9. Zhang S, Deng C, Fu BL, Yang SY, Ma L (2010) Effects of Cr doping on the electrochemical properties of Li_2FeSiO_4 cathode material for lithium-ion batteries. Electrochim Acta 55:8482–8489
10. Deng C, Zhang S, Yang SY, Fu BL, Ma L (2011) Synthesis and characterization of $Li_2Fe_{0.97}M_{0.03}SiO_4$ (M = Zn^{2+}, Cu^{2+}, Ni^{2+}) cathode materials for lithium ion batteries. J Power Sources 196:386–392
11. Hao H, Wang J, Liu J, Huang T, Yu A (2012) Synthesis, characterization and electrochemical performance of Li_2FeSiO_4/C cathode materials doped by vanadium at Fe/Si sites for lithium ion batteries. J Power Sources 210:397–401
12. Deng C, Zhang S, Yang SY (2009) Effect of Mn substitution on the structural, morphological and electrochemical behaviors of $Li_2Fe_{1-x}Mn_xSiO_4$ synthesized via citric acid assisted sol-gel method. J Alloys Compd 487:L18–L23
13. Shao B, Abe Y, Taniguchi I (2013) Synthesis and electrochemical characterization of $Li_2Fe_xMn_{1-x}SiO_4$/C ($0\le x\le0.8$) nanocomposite cathode for lithium-ion batteries. Powder Technol 235:1–8
14. Guo HJ, Cao X, Li XQ, Li LM, Li XH, Wang ZX, Peng WJ, Li QH (2010) Optimum synthesis of $Li_2Fe_{1-x}Mn_xSiO_4$/C cathode for lithium ion batteries. Electrochim Acta 55:8036–8042
15. He XG, Yang GL, Sun LQ, Xie HM, Wang RS (2010) Research on modification of cathode material Li_2FeSiO_4/C for lithium-ion battery. Chem J Chin Univ 31:2148–2152
16. Gao K, Dai CS, Lv J, Li SD (2012) Thermal dynamics and optimization on solid-state reaction for synthesis of Li_2MnSiO_4 materials. J Power Sources 211:97–102

17. Gao K, Zhang J, Li SD (2013) Morphology and electrical properties of Li_2FeSiO_4/C prepared by a vacuum solid-state reaction. Mater Chem Phys 139:550–556
18. Gao K, Dai CS, Lv J, Feng XM (2013) Effects of Carbon contents on morphology and electrical properties of Li_2MnSiO_4/C prepared by a vacuum solid-state method. Russ J Electrochem. doi:10.1134/S1023193513050066
19. Dominko R, Bele M, Gaberscek M, Meden A, Remskar M, Jamnik J (2006) Structure and electrochemical performance of Li_2MnSiO_4 and Li_2FeSiO_4 as potential Li-battery cathode materials. Electrochem Commun 8:217–222
20. Yi TF, Xie Y, Zhu YR, Zhu RS, Ye MF (2012) High rate micron-sized niobium-doped $LiMn_{1.5}Ni_{0.5}O_4$ as ultra high power positive-electrode material for lithium-ion batteries. J Power Sources 211:59–65
21. Yang JL, Kang XC, Hu L, Gong X, He DP, Peng T, Mu SC (2013) Synthesis and electrochemical performance of Li_2FeSiO_4/C/carbon nanosphere composite cathode materials for lithium ion batteries. J Alloys Compd 572:158–162
22. Liu H, Cao Q, Fu LJ, Li C, Wu YP, Wu HQ (2006) Doping effects of zinc on $LiFePO_4$ cathode material for lithium ion batteries. Electrochem Commun 8:1553–1557